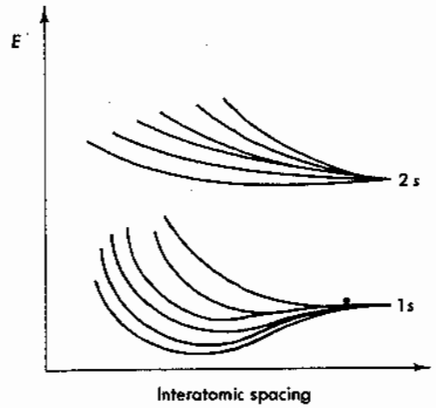

FIG. 3.5 Energy levels of a system of six similar atoms placed in a linear array.

From these considerations it is possible to understand the difference between conductors, insulators, and semiconductors. For diamond, for example, the valence band is completely filled (this fact follows also from the atomic structure of carbon and the deformation of the energy levels). The next available states are approximately 5.4 eV higher and hence cannot be reached by the electrons, with a consequent inhibition of their mobility; diamond therefore behaves as an insulator. For sodium, on the contrary, the Fermi level lies in the middle of an energy band, so that many states are available for the (3s) electron, which can move in the crystal freely;

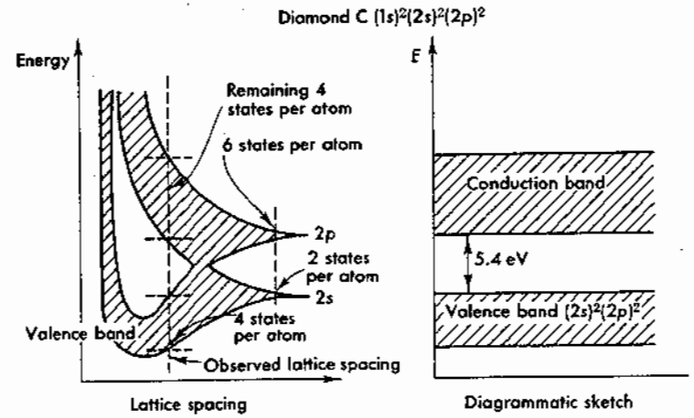

FIG. 3.6 The energy band structure of diamond (insulator) as a function of lattice spacing. The observed lattice spacing is also indicated.

sodium behaves as a conductor. Pure semiconductors, such as germanium, have a configuration such that the valence band is completely filled, but the conduction band lies fairly closely to it (0.80 eV). At high enough temperatures (that is, of the order of a few thousands of degrees), the electrons in the valence band acquire enough energy to cross the gap and occupy a state in the conduction band; when this happens the material which was previously an insulator becomes intrinsically conducting.

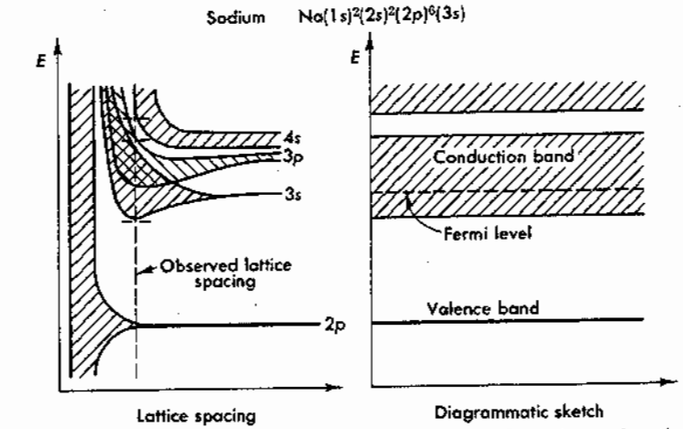

FIG. 3.7 The energy band structure of sodium (conductor) as a function of lattice spacing. The observed lattice spacing and position of the Fermi level are also indicated.

Both the electric and thermal conductivity of a solid depend on the density and mobility of the free electrons. Completely analogous to the motion of electrons is the motion of "holes"; holes can be thought of either as "vacancies" in an almost-filled band, or as electrons with negative effective mass.† Due to their thermal energy, the carriers have a random motion characterized by $(3/2)kT = E = m^*v^2/2$. When electric potential or temperature gradients are applied, a drift velocity is superimposed on the random motion of the carriers in such a direction as to establish a steady state current flow.

2. Thermionic Emission of Electrons from Metals

It is well known that when a metal is heated to high temperatures it emits electrons, as in the case of the filament of an electron tube. To ob-

† This can be seen from Eq. 1.9 and the negative curvature of some parts of the $E(k)$ curve of Fig. 3.4a.

From "Experiments in Modern Physics" Adrian C. Melissinos Academic Press 1966. Chapter 3, section 2 Thermionic Emission & Electrons from Metals pp 65-80

serve thermionic current, both the emitter and detector are placed in an evacuated vessel and electric field acceleration is provided. However, the electric fields present and the geometrical configuration of filament and cathode complicate the interpretation of the emission process itself. We will proceed by first deriving the expression for the emitted current density (Richardson's equation) and the modifications needed when an accelerating or decelerating potential is applied; next we will give the expression for the space charge limited current† (Child's law) and consider the experimentally measurable quantities; finally, the equipment and experimental procedure will be discussed and analysis of specific data will follow.

2.1 Derivation of Richardson's Equation

Let us first consider the potential in the vicinity of a metal boundary. We assume that the potential ϕ inside the metal is constant (hence $E = 0$), but at the boundary proper, there must exist strong forces if the electrons are to remain contained; Fig. 3.8a shows such a square barrier potential. However, an electron which is outside a plane conducting surface is attracted to it by the force exerted between itself and its fictitious image. (The image is introduced so that for $z \geq 0$ the potential satisfies both Laplace's equation and the boundary conditions on the metal surface, Fig. 3.8b). Since $F = e^2/(4\pi\epsilon_0 4z^2)$, it follows that

$$V = -\int E\,dz = -\frac{e}{16\,\pi\epsilon_0 z} \tag{2.1}$$

Combining Eq. 2.1 with the square barrier of Fig. 3.8a, we obtain the more

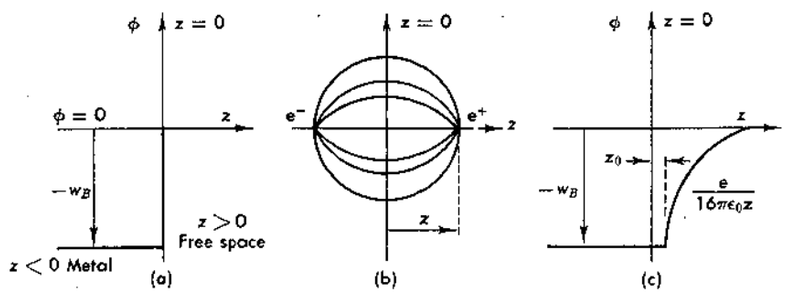

Fig. 3.8 Idealized potentials to which an electron near the surface of a metal is subjected. (a) Square barrier at metal boundary. (b) The lines of force between an electron and its image. (c) The resulting potential from combining (a) and (b).

† See, for example, N. H. Frank, *Introduction to Electricity and Optics*. New York: McGraw-Hill, 1950, p. 220.

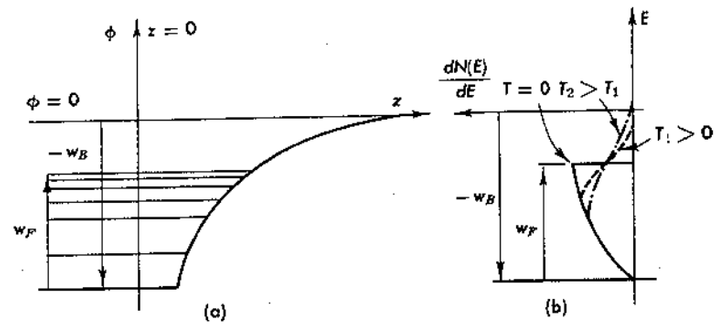

Fig. 3.9 The energy distribution of electrons inside a metal with respect to the potential barrier. (a) The ordinate gives energy, whereas the abscissa gives the distance from the boundary; the density of horizontal lines is proportional to the number of electrons that have this particular energy. (b) The density of occupied electron states versus energy; this is shown for different Temperatures, T.

realistic image field barrier shown in Fig. 3.8c. The Coulomb potential has been cut off at $z = z_0$ where $V(z_0) = -e/(16\,\pi\epsilon_0 z_0) = w_B$; w_B is the depth of the potential well in which the *free* electrons are bound; or in band structure terminology, the potential energy of the bottom of the conduction band. In Fig. 3.9a the density of states inside the potential well is sketched by using Eq. 1.4; in Fig. 3.9b a plot of the density (abscissa) for various temperatures is given. Thus, free electrons with energy $E > w_B$ can overcome the boundary and will escape if their direction of motion is towards the boundary. As is usually done in escape problems, we calculate the number of electrons within a right cylinder of unit area, and of height v_z, with $v_z^2 > 2w_B/m$ (this gives the number of electrons that reach unit area in unit time and have the appropriate velocity component). Thus

$$J = eN(\text{escape/sec cm}^2) = e\int_{v_z=\sqrt{(2w_B/m)}}^{+\infty} \frac{dN(v_z)}{dv_z}\,v_z\,dv_z$$

the distribution function $dN(v_z)/dv_z$ has been given in Eq. 1.4a, and for most values of T the exponential is very small (at $T = 3000°$ K the exponential is e^{-8}) so that

$$\ln(1+x) = x - \tfrac{1}{2}x^2 + \tfrac{1}{3}x^3 - \tfrac{1}{4}x^4 + \cdots$$

and thus

$$J = e\frac{4\pi m^2 kT}{h^3}\int_{\sqrt{(2w_B/m)}}^{+\infty} v_z \exp\left(w_F - \tfrac{1}{2}mv_z^2\right) dv_z$$

We make the following change of variables

$$u = \frac{w_F - \frac{1}{2}mv_z^2}{kT} \qquad du = -\left(\frac{mv_z}{kT}\right) dv_z$$

and

$$v_z = \left(\frac{2w_B}{m}\right)^{1/2} \rightarrow u = \frac{w_F - w_B}{kT}$$

$$v_z = +\infty \rightarrow u = -\infty$$

so that

$$J = -\frac{4\pi mek^2T^2}{h^3} \int_{(w_F - w_B)/kT}^{-\infty} e^u \, du$$

giving Richardson's equation,

$$J_0 = A_0T^2 \exp(-e\phi/kT) \tag{2.2}$$

with

$$A_0 = \frac{4\pi mek^2}{h^3} = 1.2 \times 10^6 \text{ amp/m}^2\text{-deg}^2$$

and

$$\phi = \frac{w_B - w_F}{e}$$

is the work function in volts.

We have thus obtained Richardson's equation, which shows that the thermionic emission is dominated by an exponential temperature dependence. This dependence is so strong that the T^2 factor is completely masked and cannot be directly verified by experiment. Furthermore, the constant A_0 observed experimentally is seldom in agreement with the theoretical value. This is due to the simple assumptions used in the derivation and the neglect of such effects as:

(a) Temperature dependence due to variations in ϕ. Because if

$$\phi = \phi_0 + aT,$$

then

$$J = (A_0e^{-ae/k}) T^2 \exp(-e\phi_0/kT)$$

where the exponential can easily alter the value of A_0 by factors of 2 or larger.

(b) Quantum-mechanical reflections of the electrons at the surface. Such reflections will be equivalent to a modification of the barrier potential assumed.

(c) Nonuniformity of the emitting surface, since we really measure

$$J = A_0T^2 \sum_i \exp(-\phi_i e/kT)$$

We can now consider the modifications to the emission-current density J_0 due to the application of external fields. The two cases of a retarding field and of an accelerating field are sketched in Figs. 3.10a and 3.10b, respectively.

For a retarding field, the barrier potential that the electron has to overcome is increased by the whole amount of the retarding potential V_0, so that

$$J' = AT^2 \exp\left(-\frac{e(\phi + V_0)}{kT}\right) = J_0 \exp\left(-\frac{V_0e}{kT}\right) \tag{2.3a}$$

hence an exponential reduction of the current with increasing retarding potential.

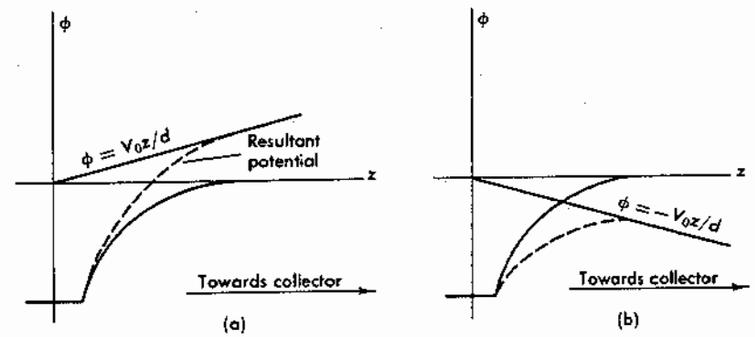

FIG. 3.10 The potential seen by an electron inside a metal when an external field is applied. (a) Retarding field. (b) Accelerating field.

An accelerating field, on the other hand, as can be seen from Fig. 3.10b, can lower the potential barrier by only a small amount. For plane geometry the resultant potential is

$$V = -\frac{e}{16\pi\epsilon_0 z} - \frac{V_0 z}{d}$$

which has a maximum at

$$z_{\max} = \sqrt{\frac{ed}{16\,\pi\epsilon_0 V_0}}$$

with the value

$$V_{\max} = -2\sqrt{\frac{V_0 e}{16\,\pi\epsilon_0 d}}.$$

The barrier seen by the electrons is

$$e\phi = -V_{\max} - w_B = -w_B + 2\sqrt{\frac{V_0 e}{16\,\pi\epsilon_0 d}}$$

and

$$J_s = J_0 \exp\,[0.44(E^{1/2})/T], \tag{2.3b}$$

where E is the electric field in volts per meter (for a plane diode $E = V_0/d$), and J_s is the saturation current. Because of the factor $0.44/T$, the increase in emission current is very small; on a semilog plot it is proportional to the square root of the applied accelerating potential.

2.2 Child's Law and the Measurable Quantities in the Thermionic Emission Experiment

As mentioned before, the measured values of the thermionic current are affected by space-charge effects; that is, the emitted electrons form a sheath of negative charge in the vicinity of the cathode, inhibiting further emission. It is therefore necessary to apply a positive potential to accelerate the electron toward the anode and so reduce the space-charge layer.

By solving Poisson's equation in the space between cathode and anode and taking account of the dynamical equilibrium, we obtain expressions for the current density against voltage when accelerating fields are applied. These expressions depend on geometry and are, for a plane diode,

$$J = \frac{4\epsilon_0}{9}\sqrt{\frac{2e}{m}}\,V_0^{3/2}\,d^{-2} \tag{2.4a}$$

and for a cylindrical diode

$$J_a = \frac{4\epsilon_0}{9}\sqrt{\frac{2e}{m}}\,V_0^{3/2} r_a^{-2}\beta^{-2}, \tag{2.4b}$$

where MKS units are used and J or J_a is the current density at the *anode*. Here V_0 is the applied potential, d the anode-cathode separation for the plane diode, and r_a the anode radius for the cylindrical diode; β is a correction coefficient which is a function of (r_c/r_a) and can be found in the literature.† Equations 2.4 are known as "Child's law."

† Langmuir and Blodgett, "Currents Limited by Space Charge Between Coaxial Cylinders," *Phys. Rev.* **22**, 347 (1923).

As the voltage is further increased, J tends toward and finally reaches the saturation-current value given by Eq. 2.3b. We can now see what the measurable quantities are and what experimental procedure to follow.

(a) At fixed filament temperature, the anode current is measured against accelerating potential well into the saturation region. (A family of such curves is shown in a log-log plot in Fig. 3.14.) From the space-charge region we can verify Eqs. 2.4, the $V_0^{3/2}$ dependence, and obtain a value for e/m.

From the saturation region we can verify Eq. 2.3b, the $E^{1/2}$ dependence of the current density, and obtain the zero field density $J_0(T)$. It is then possible to check Eq. 2.2 (see Fig. 3.16) and find a value for the coefficient $e\phi/k$ of the exponent (hence the work function), and for the coefficient A_0.

(b) At fixed filament temperature the anode current is measured as a function of decelerating potential. One can verify the exponential dependence of J' and determine the coefficient e/kT of the exponent (Eq. 2.3a). In principle one can again determine $J_0(T)$, but values obtained from the saturation current are more accurate.

As is clear by now, a knowledge of the filament temperature is needed; the region of interest for pure tungsten (the cathode material used in this experiment) is in the region of 2000° K where thermionic emission currents can be reasonably detected. The measurement of the temperature cannot be made very accurately and is based on the change in resistivity of tungsten, or by using an optical pyrometer. The special tube used in this laboratory has a small hole in the anode so that the central part of the filament can be viewed for the optical determination of the temperature.

When the change in resistivity is used, it is important to be able to separate the effects due to lead resistance and filament resistance. While the lead resistance should remain constant, nevertheless it changes, since the leads become heated by conduction from the filament. It is also important to determine correctly the room temperature resistance, since in the measuring process the filament becomes heated. In addition, the filament itself is not at uniform temperature throughout its length, but is lower by a factor of $\frac{1}{3}$ at its terminal points. A correction for this effect can be included in the data.

2.3 Thermionic Emission Experiment and Results

In this laboratory a specially constructed cylindrical diode is used. The FP-400 tube manufactured by the General Electric Company† (Fig. 3.11) is a high-vacuum tube with a pure tungsten filament. Some relevant

† "The manufacture of these tubes has recently been discontinued; however a limited supply is available from G. J. Baberich, P. O. Box 118, Berkeley Heights, New Jersey. A possible substitute would be a diode such as 5U4."

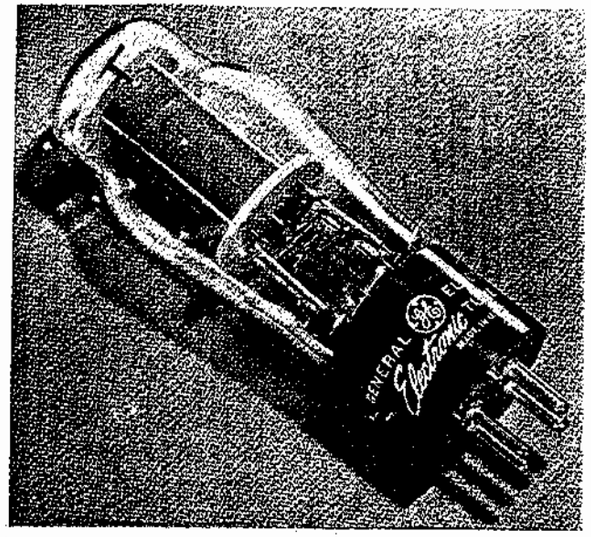

FIG. 3.11 Photograph of the General Electric FP-400 vacuum tube appropriate for thermionic emission measurements.

data† are as follows:

Pure tungsten filament, length	3.17 cm
diameter	0.013 cm
Anode, Zr coated Ni, I.D.	1.58 cm
Average lead resistance	0.08 ohms
Maximum filament voltage	4.75 V
Maximum filament current	2.5 amp
Maximum anode voltage	125 V
Maximum anode current	0.055 amp
Maximum anode dissipation	15 W

The resistivity of tungsten is 5.64×10^{-6} ohms/cm at 27° C.

The circuit diagram is shown in Fig. 3.12. Filament heating is provided by a d-c balanced supply to minimize potential differences along the filament. The shunt and potentiometer shown in the filament circuit are used for resistivity measurements. The configuration shown in the figure is best suited for the application of accelerating potentials; for decelerating potentials a galvanometer must be introduced in the anode branch. In

† From the manufacturer's data sheet.

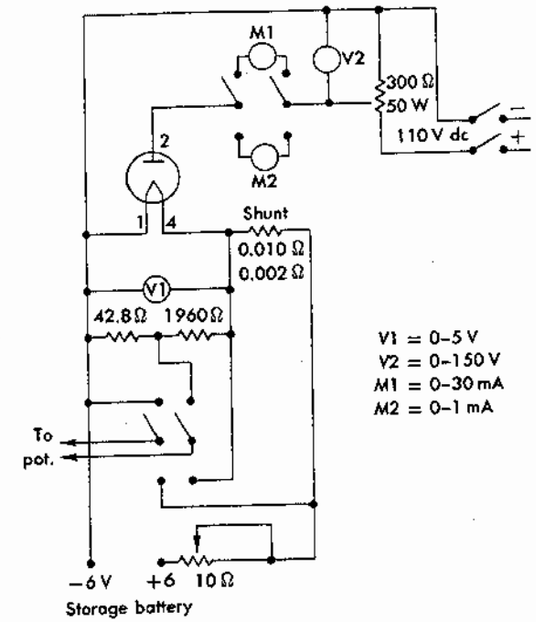

FIG. 3.12 Circuit diagram for thermionic emission experiment.

the latter instance voltage gradients along the filament become a serious consideration, and knowledge of the correct retarding potential is difficult to achieve unless a switching technique is used for filament heating.

When taking data, the maximum filament rating of 4.5 V should not be exceeded. Information necessary for the temperature determination is given in Fig. 3.13, which is a plot of the ratio of the resistivity of tungsten (W), obtained from independent calibration.†

Data obtained by a student‡ are shown in Fig. 3.14, which is a log–log plot of anode current against anode voltage. Since the geometry is cylindrical, we obtain the saturation current from Eq. 2.4b

$$I_s = l\frac{8\pi\epsilon_0}{9}\sqrt{\frac{2e}{m}}V_0^{3/2}r_a^{-1}\beta^{-2} \tag{2.4c}$$

† Worthington and Forsythe, *Astrophys. J.*, **61**, 146–185 (1925) contains an extensive discussion of the properties of tungsten and corrections for lead losses of tungsten filaments.

‡ D. Kohler, class of 1962.

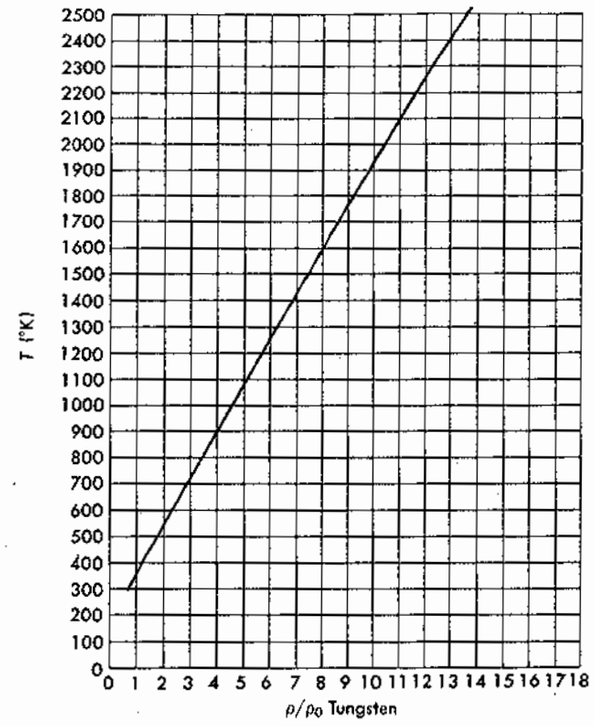

FIG. 3.13 Relative resistivity of tungsten.

where l is the length of the filament; for this particular tube the constant β^{-2} has the value 0.93. In the space-charge region, the plots are indeed straight lines and their slope is

$$\frac{\Delta \log I}{\Delta \log V} = 1.49 \pm 0.02$$

in agreement with the prediction of Eqs. 2.4. If we attempt, however, to obtain e/m using Eq. 2.4c, and accept as the current $I = 0.041 \times 10^{-3}$ amp at 1 V, the result is

$$e/m = 1.07 \times 10^{11} \text{ coul/kg}$$

while the true value is $e/m = 1.76 \times 10^{11}$ coul/kg. This discrepancy is not surprising since only a fraction of the filament length l contributes effectively to the emission process; this is due to both thermal and collection end-effects.

To obtain the filament temperature, first the resistance of room temperature was measured and extrapolated to zero current (Fig. 3.15), with the result $R' = 0.285$ ohms; next the filament resistance was calculated from its geometrical dimension and found to be $R_f = 0.135$ ohms, so that the lead resistance must be $R = R' - R_f = 0.15$ ohm. From the measurements of R' it is then possible to obtain the corresponding temperature, which has been used to label the curves of Fig. 3.14.

Once the temperature is known, the zero field current I_0 can be obtained from the saturation current I_s through Eq. 2.3b; the correction is in general small. Since the geometry is cylindrical,

$$V = \int \mathbf{E} \cdot d\mathbf{r} = (Er) \ln \frac{r_a}{r_f}$$

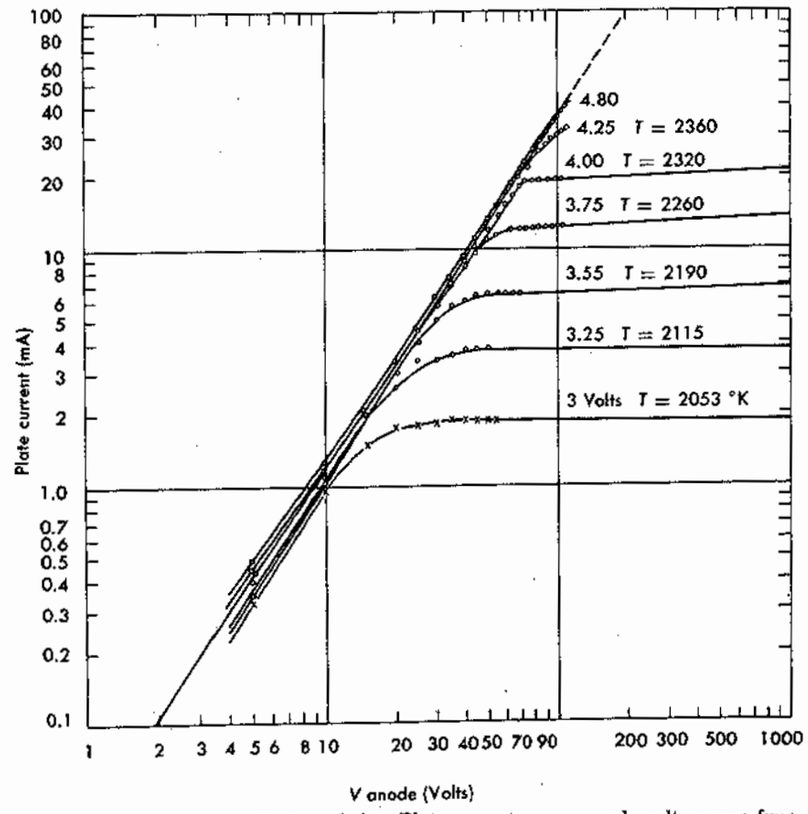

FIG. 3.14 Data on thermionic emission. Plate current versus anode voltage as a function of filament temperature.

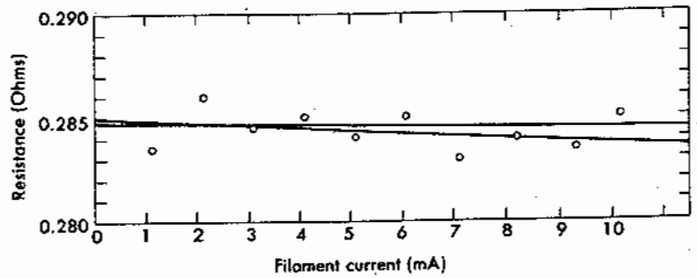

FIG. 3.15 "Cold" resistance of tungsten filament and leads.

hence

$$E = \frac{V}{r} \ln \frac{r_f}{r_a}.$$

The results are summarized in Table 3.1, where $J_0 = I_0/(2\pi r_c l)$ is the thermionic emission current density at the cathode.

TABLE 3.1
DATA OBTAINED FROM THERMIONIC EMISSION EXPERIMENT

Filament voltage	3	3.25	3.5	3.75	4.0	4.25
T (°K)	2053	2115	2190	2260	2320	2360
I_e (ma) at 110 V	2.0	3.7	6.8	12.5	20.2	33.8
I_0 (ma)	1.76	3.28	6.03	11.13	18.05	30.25
J_0/T^2 (amp deg^{-2}m^{-2})$\times 10^{-4}$	0.324	0.582	0.975	1.69	2.52	4.18

A plot of the values of J_0/T^2 against $1/T$ in a semilog plot is given in Fig. 3.16; from it a slope

$$\frac{e\phi}{k} = 37{,}500° \text{ K}$$

is obtained, hence

$$\phi = 3.22 \text{ V}$$

Similar but more precise measurements by Langmuir and Jones† yield $\phi = 4.52$ V, which is within the accepted value for the work function of tungsten. It is clear that values of A_0 obtained from these data depend

† From General Electric data sheet for FP-400.

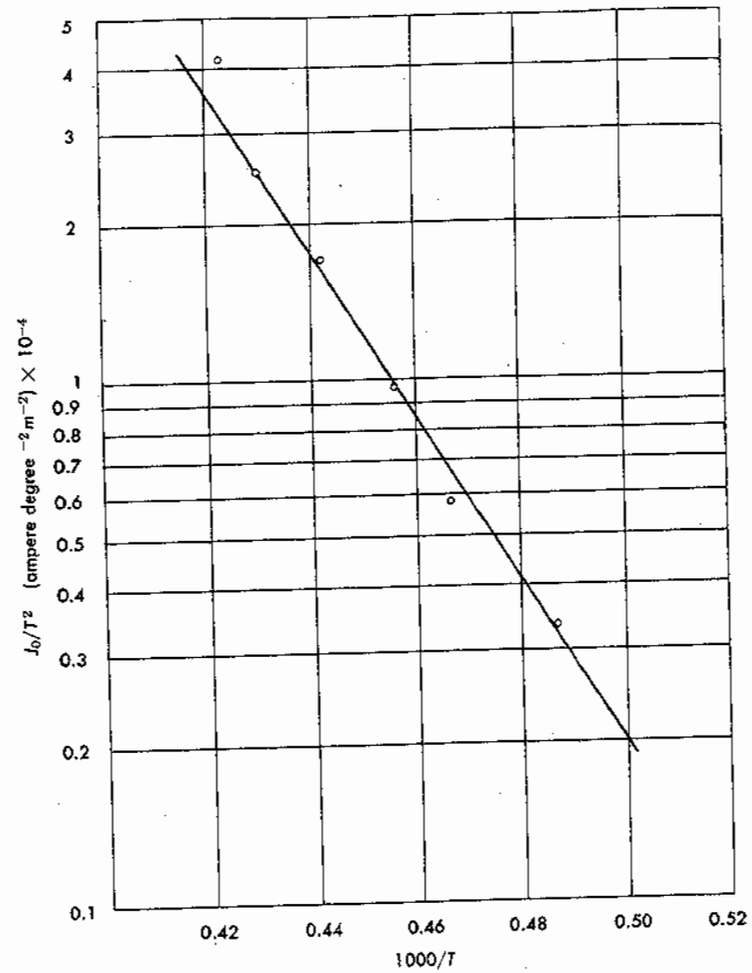

FIG. 3.16 Determination of the work function of tungsten. The saturation current density J_0/T^2 is plotted versus $1/T$ from the data of Fig. 3.14.

in a very sensitive manner on the slope of the linear fit in Fig. 3.16. For example, using these data, we obtain $A_0 = 33.5$ amp/deg^2-m^2 which is orders of magnitude off from the accepted value†

$$A_0 = 60 \times 10^4 \text{ amp/deg}^2\text{-m}^2$$

† This differs from the theoretical value by a factor of 2, attributed to reflections at the surface.

On the other hand, if Langmuir's value of $\phi = 4.52$ V is accepted for the slope, the data of Fig. 3.16 yield a more reasonable value:

$$A_0 = 176 \times 10^4 \text{ amp/deg}^2\text{-m}^2.$$

When a retarding potential is applied, measurements with the present setup are more difficult because of the effect of voltage gradients along the filament; also space-charge effects are still quite pronounced for anode currents of the order of 10^{-5} amp so that only data beyond this point must be considered. For such measurements see Harnwell and Livingood, *Experimental Atomic Physics*, page 210.

2.4 The Stefan-Boltzmann Law

With the data obtained from the thermionic emission experiment, it is possible to verify the Stefan-Boltzmann law. This law, which can be derived on thermodynamic arguments, states that the total energy radiated per second by a black body of unit surface area is proportional to the fourth power of the temperature.

$$E = \sigma T^4 \tag{2.5}$$

where E is the total power radiated from unit area, T the temperature in degrees Kelvin, and σ is Stefan's constant.

By integrating Planck's radiation law over all wavelengths, Eq. 2.5 can be obtained. Since the energy density u_ν for a frequency ν is

$$u_\nu \, d\nu = \frac{8\pi h}{c^3} \frac{\nu^3}{\exp(h\nu/kT) - 1} \, d\nu \tag{2.6}$$

$$u = \int_0^\infty u_\nu \, d\nu = \frac{8\pi k^4 T^4}{h^3 c^3} \int_0^\infty \frac{z^3}{e^z - 1} \, dz = \frac{8\pi k^4}{h^3 c^3} \frac{\pi^4}{15} T^4 \tag{2.7}$$

If the total power emitted by a black body per unit area is E, the energy density when in equilibrium is

$$u = (4/c) E$$

so that

$$E = \frac{c}{4} \frac{8\pi^5 k^4}{15 h^3 c^3} T^4 \tag{2.8}$$

and substitution of the constants in Eq. 2.8 gives the experimentally observed value of $\sigma = 5.64 \times 10^{-8}$ joules m^{-2} deg^{-4} sec^{-1}.

If it is then assumed that the energy loss of the filament through conduction in the leads is small, the radiated power is given

$$P = I^2 R_f$$

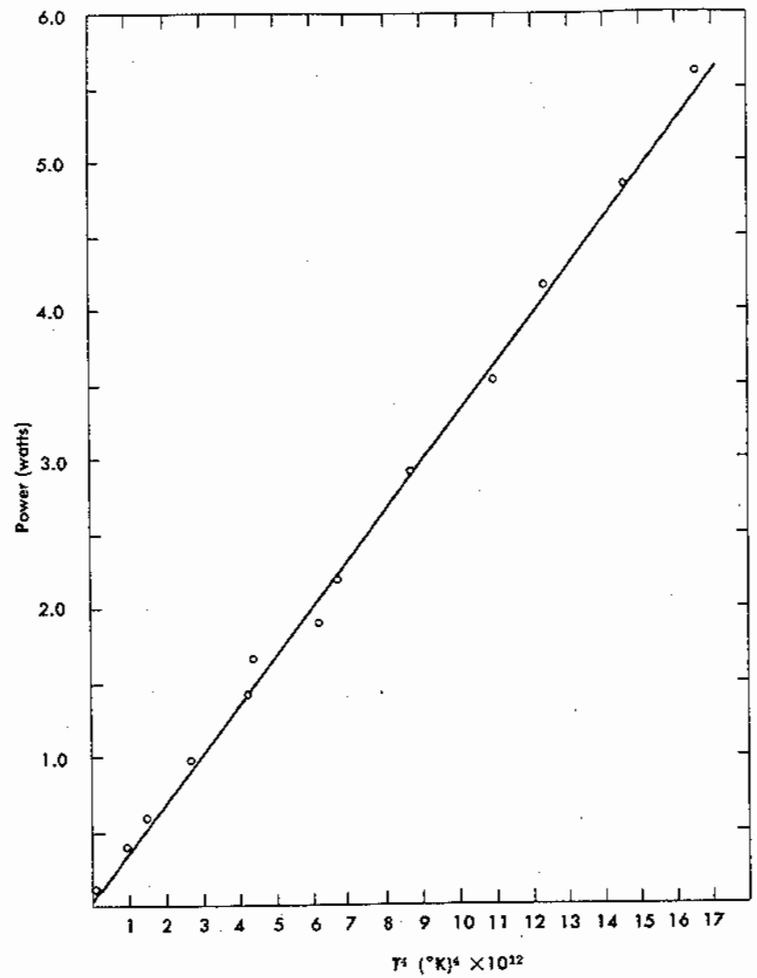

FIG. 3.17 Verification of Stefan's law. Plot of radiated power versus filament temperature.

A plot of P against T^4 as obtained by a student† is given in Fig. 3.17. The best fit to his data gives

$$P \propto T^{4.08}$$

† D. Owen, class of 1963.

and for Stefan's constant, $\sigma = 2.7 \times 10^{-8}$ joules m^{-2} deg^{-4} sec^{-1} which is of the correct order of magnitude, and smaller† than σ.

In concluding, we note that our results have confirmed the exponential dependence on temperature of the thermionic current (Richardson's equation), and the phenomena of space charge. Also, qualitative agreement has been achieved with the accepted values of the parameters involved; similarly, agreement has been achieved for Stefan's law.

3. Some Properties of Semiconductors

3.1 General

We have seen in the first section how a free-electron gas behaves, and what can be expected for the band structure of a crystalline solid. In the second section we applied the principle of free-electron gas behavior to the emission of electrons from metals, and in the present section we will apply both principles to the study of some properties of semiconductors which can be verified easily in the laboratory.

As mentioned before, a semiconductor is a crystalline solid in which the conduction band lies close to the valence band, but is not populated at low temperatures; semiconductors are unlike most metals in that both *electrons* and *holes* are responsible for the properties of the semiconductor. If the semiconductor is a pure crystal, the number of holes (positive carriers, p) is equal to the number of free electrons (negative carriers, n), since for each electron raised to the conduction band, a hole is created in the valence band; these are called the *intrinsic* carriers.

All practically important semiconductor materials, however, have in them a certain amount of impurities which are capable either of donating electrons to the conduction band (making an n-type crystal) or of accepting electrons from the valence band, thus creating holes in it (making a p-type crystal). These impurities are called *extrinsic* carriers; in such crystals $n \neq p$.

Let us then first look at the energy-band picture of a semiconductor as it is shown in Fig. 3.18; the impurities are all concentrated at a single energy level usually lying close to, but below, the conduction band. The density of states has to be different from that of a free-electron gas (Eq. 1.4 and Fig. 3.2a) since, for example, in the forbidden gaps it must be zero; close to the ends of the allowed bands it varies as $E^{1/2}$ and reduces to zero on the edge. On the other hand, the Fermi distribution function, Eq. 1.3, remains the same. The only parameter in this function is the Fermi energy, which can be found by integrating the number of *occupied* states (Fermi function

† Note that the tungsten filament is not a perfect black body; the emissivity of a hot tungsten filament is usually taken as one third.

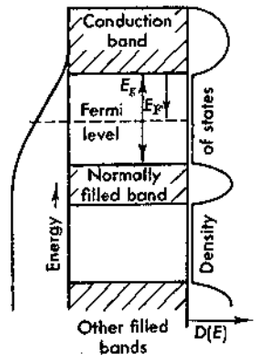

FIG. 3.18 Energy band structure of a semiconductor without impurities. On the left-hand side the Fermi distribution for a free-electron gas is shown; on the right-hand side the actual density of states $D(E)$ is shown.

times density of states) and setting it equal to the electron density. It is clear, however, that if we are to have as many empty states in the valence band as occupied ones in the conduction band, the Fermi level must lie exactly in the middle of the forbidden gap† (because of the symmetry of the trailing edge of the distribution). In Fig. 3.18, the density of states is shown to the right and the Fermi distribution function to the left. We measure the position of the Fermi level *from the conduction band* and define it by E_F; the exact value of E_F is

$$E_F = -\frac{E_g}{2} + kT \ln \left(\frac{m_h^*}{m_e^*}\right)^{3/4} \tag{3.1}$$

Since the Fermi level lies below the conduction band, E_F is a *negative* quantity; E_g is the energy gap always taken positive and m_h^* and m_e^* are the effective masses of holes and electrons, respectively. If w_C and w_F stand for the actual position of the conduction band and Fermi level above the zero point energy, then

$$w_F = w_C + E_F$$

To find the number of electrons in the conduction band (or holes in the valence band) we simply substitute Eq. 3.1 for w_F into Eq. 1.4, multiply by the density of states, and integrate over w from $w = w_C$ to $+\infty$. When, however, the exponent

$$-(w_F - w) \approx \frac{E_g}{2} + E \gg kT \tag{3.2}$$

the Fermi distribution degenerates to a Boltzmann distribution. (Here E is the energy of the electrons as measured from the top of the conduction band; obviously it can take either positive or negative values.) With this

† If the effective masses of p- and n-type carriers are the same.